Composite Structures 322 (2023) 117343

Contents lists available at ScienceDirect

Composite Structures

journal homepage: www.elsevier.com/locate/compstruct

# Multi-scale procedure for the mechanical analysis of composite laminate structures considering mixed boundary conditions

Francesc Turon [a,b,*], Fermin Otero [a,b], Xavier Martinez [a,b]

[a] Centre Internacional de Metodes Numerics a l'Enginyeria (CIMNE), Campus Nord UPC, Barcelona, 08034, Spain
[b] Departament de Ciència i Enginyeria Náutiques (DCEN), Universitat Politècnica de Catalunya · BarcelonaTech (UPC), Facultat de Nàutica de Barcelona (FNB), Plà de Palau 18, Barcelona, 08003, Spain

ARTICLE INFO

*Keywords:*
Multi-scale
Composite
Laminate
Numerical homogenization
Shell theory

ABSTRACT

This paper presents a multi-scale procedure for the study of flat composite structures with discontinuities. In this procedure, the structure is solved using shell elements while the laminate performance and the structural discontinuities (e.g. connections or change in the laminate thickness) are analysed with a subscale model made with solid 3D elements. The kinematics of both models are coupled following the Kirchhoff–Love theory. This coupling is used during the homogenization procedure where the characteristic behaviour of the different micro-models is obtained. Periodical boundary conditions are used for the laminates whereas a combination between periodical and linear boundary conditions are used for the discontinuities. The proposed procedure allows to reproduce accurately the structure elastic behaviour, as well as the stress and strain states in regions with discontinuities, which until now could only be accurately simulated by means of expensive numerical models using volumetric solid elements.

## 1. Introduction

In recent decades the size of structures designed and built with composite laminates has grown significantly. In addition, the increasingly widespread use of this kind of material is also leading to more sophisticate structures. In particular, some of these structures are made of complex laminates that are designed to suit better their mechanical needs [1]. The hull of larger vessels, structural components for civil construction, the blades of wind turbines, and larger part of airplane fuselage are examples of these structures [2,3].

Most composite laminate structures have connections, transitions zones and internal microstructures that increase the complexity of the structures morphology [4,5]. The presence of such discontinuities increases the challenge of the structural analysis. When the finite element method is used to solve the mechanical problem there are commonly two options to discretize the structure, i.e. volumetric solid elements and superficial shell elements. Each ones having its advantages and disadvantages, as it is described hereafter [6].

A detailed finite element mesh with solid elements allows to capture the tensional and deformational state in each part of the composite laminate. Moreover, this kind of elements are capable of reproducing the stress states that occur in areas of transition, reinforcement, union and overlapping. Nonetheless, a solid elements mesh has higher computational cost due to the number of elements needed to discretize the geometry. In example, to correctly capture the evolution of the stresses in the composite it is necessary to define several elements thought the thickness direction. Considering that a conventional laminate is made of dozens of layers, the necessary number of elements increase steeply. Manage such large meshes is a disadvantage in terms of computational cost, and also in the pre- and post-process tasks.

The problem related to the high computational cost associated with solid finite elements can be solved by using shell finite elements. In this case, all the layers of the laminate are concentrated in its reference plane [7] which is then discretized as a surface, thus drastically reducing the computational cost. However, grouping all the layers in a single reference surface entails, in some cases, loss of accuracy. Plate theories, such as Kirchhoff-Love's, Reissner-Midlin's [6] or Zigzag [8] approximate the real deformation field of the laminate by assuming numerous simplifications. Alternatively, novel and interesting approaches have been recently proposed, as an instance, the method proposed by Carrera et al. [9], which uses a global shell model of the structure to obtain a local three dimensional representation of the stress–strain distribution in each one of its elements. For continuous laminates, all these approaches achieve good results, being able to give the resulting average tension on each layer. Nevertheless, they cannot capture the concentrations of stresses and deformations generated in zones of transition and irregularities.

* Corresponding author.
*E-mail address:* fturon@cimne.upc.edu (F. Turon).

https://doi.org/10.1016/j.compstruct.2023.117343
Received 13 January 2023; Received in revised form 22 June 2023; Accepted 7 July 2023
Available online 18 July 2023

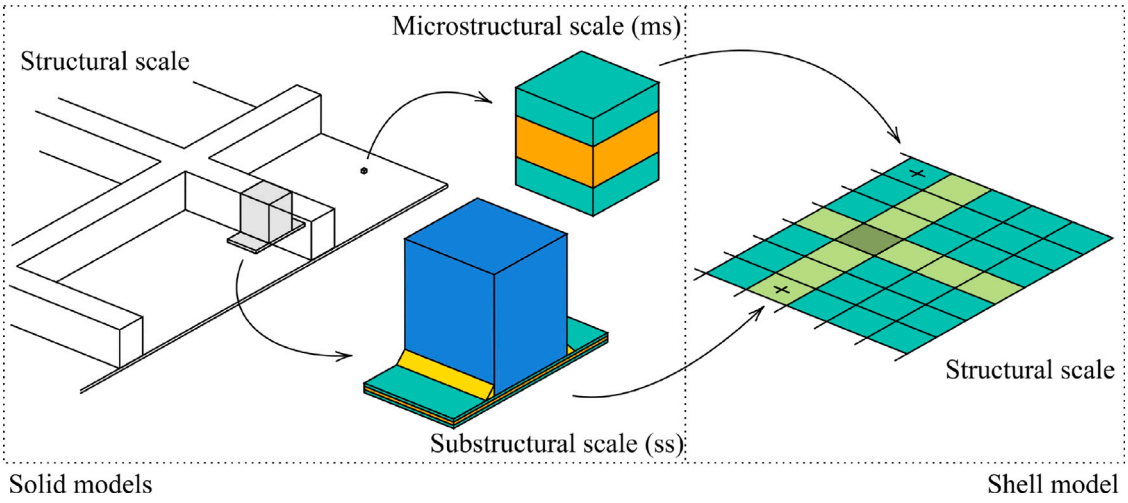


**Fig. 1.** Representation of the different scales considered and the path followed during the problem definition.

Several authors have proposed formulations that, using multiscalar approaches, couple models with different finite elements, for example shells and volumetric solids elements, in order to benefit from the advantages provided by each one of them. Most of these frameworks differ among them on the displacement field applied at the boundaries between the elements, required to couple both scales. Gruttmann and co-authors [10] use the kinematic definition established by the Reissner–Mindlin plate theory while imposing a zero stress in the perpendicular direction of the plane on the upper and lower faces. Massart et al. [11] rely on Kirchhoff's kinematics introducing the periodical boundary condition in a similar way as does Mallikarachchi [12]. More complex formulations such as the one developed by Helfen in [13] take into account the thickness variation of the laminate. The authors Geers [14] and Coenen [15] also rely on the Reissner–Mindlin formulation but using the second-order homogenization procedure previously proposed by Kouznetsova [16]. Alternatively other authors rely on the asymptotic homogenization for approximating the shell kinematics, see Huang and Cai et al. [17,18], respectively. This approach aims to enrich the kinematics of the original plate theories by adding among others the out-of-plane phenomena. The precision of the results obtained applying the described formulations to a composite laminate is demonstrated by numerous numerical analyses. However, these formulations, and the analyses conducted with them, are limited to laminates with a constant configuration along the whole structure.

The methodology proposed in this work aims to reduce the computational cost of simulations while maintaining the level of precision provided by volumetric solid models. The proposed approach consists in simulating the structure using shell elements and obtaining the mechanical performance of these shell elements from their numerical 3D solid models representation. This is graphically presented in Fig. 1, in which are introduced the different scales and models considered. On the left it is shown the dimensional scales involved in the numerical simulation while on the right it is shown the resultant equivalent shell model that gathers the different scales considered.

In the structure shown in Fig. 1 it is possible to identify three different dimensional scales i.e. structural, substructural and microstructural. In the proposed approach, the substructural scale is defined as a discontinuity in the structure that is repeated along the geometry. On the other hand, the microstructural scale corresponds to the periodical internal structure of the laminate. The constitutive behaviour of the shell elements, at the structural level, are characterized with a homogenization procedure that use the substructural and microstructural scales (see Section 2.2). The latter two subscales are modelled using volumetric solid elements, which allow to fully reproduce the behaviour of discontinuities and internal laminate structures.

In addition, this work studies the boundary conditions necessary to carry out the homogenization process to characterize the substructural scale. The proposed boundary conditions are a combination of free, linear and periodic conditions applied on the contour faces of the models. They allow to take into account the loss of periodicity as well as the scale separation concept [19], which is one of the main hypothesis in which a computational multi-scale homogenization procedure is based. Moreover, the presented methodology relies on a second order homogenization formulation [16] to develop a novel homogenization procedure in order to obtain the effective behaviour of the substructural scale.

Current manuscript is divided as follows. In the first section the kinematic coupling between the models of both scales is introduced. Then this coupling is applied to the homogenization of continuous and discontinuity laminate regions. The implementation process is briefly explained afterwards. Finally an example is shown where a rectangular laminated sample with a discontinuity in the center is studied. This example is also used to validate the procedure proposed.

The mathematical notation used is the following. Scalars, vectors, unit vectors, second and n-order tensors have been denoted as $a$, $\vec{a}$, $\hat{a}$, $\mathbf{A}$ and ${}^{n}\mathbf{A}$ respectively. Using the Cartesian reference system, with $\hat{e}_i$ where $i = 1, 2, 3$, and the Einstein notation, the dot products shown correspond to tensor-tensor, tensor-vector and vector-tensor-vector as $\mathbf{A} \cdot \mathbf{B} = A_{ij} B_{jk} \hat{e}_i \hat{e}_k$, $\mathbf{A} \cdot \vec{b} = A_{ij} b_j \hat{e}_i$, $\vec{a} \cdot {}^{3}\mathbf{B} \cdot \vec{c} = a_i B_{ijk} c_k \hat{e}_j$, respectively.

## 2. Multi-scale procedure proposed

The current section describes the multi-scale approach developed in this work. The objective is to efficiently take into account the stiffness contribution of the micro and substructural scales at the structural scale level.

In order to relate the scales involved in the problem, it is necessary to establish the kinematic relationship that exist between them. The proposed relationship must consider the different finite element technologies used in each scale. Due to the nature of the shell-like problem at the structural scale, a second order multi-scale framework is formulated. However, specific boundary conditions are applied to solve the subscales boundary value problem in order to account for the loss of periodicity.

The procedure proposed to couple both scales is schematically presented in Fig. 2. The characteristic mechanical behaviour of the substructure and microstructure, at the structural level, is obtained with a numerical homogenization. The **ABD** constitutive matrix, which relates the force and moment per unit length with the strains of the shell, is obtained by solving the subscale models applying all possible

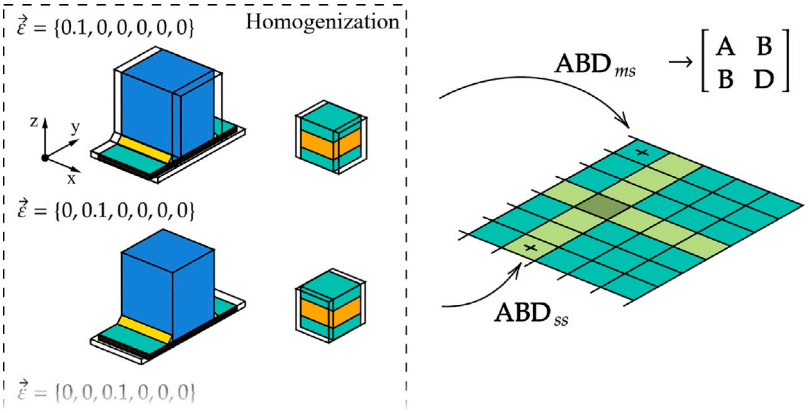


**Fig. 2.** Definition of the ABD shell constitutive matrices following the homogenization procedure.

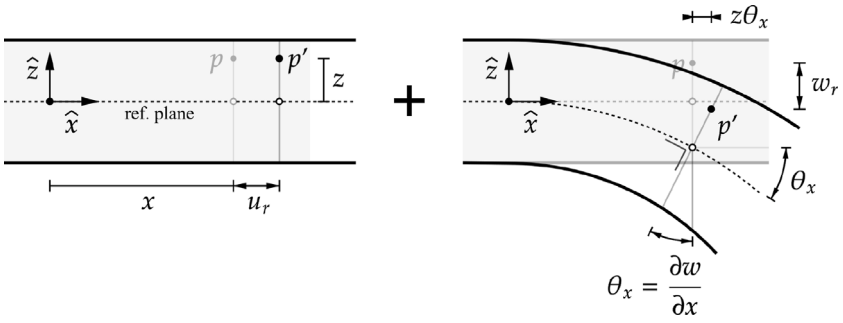


**Fig. 3.** Deformation of the laminate according to the KL plate theory.

pure strain states (strain tensors with a unit value in one direction, and zero in the rest). This procedure, known as homogenization, is similar to the one defined to obtain the tangent constitutive tensor by numerical derivation in [20]. Finally, the shell elements used at the structural problem are defined using the obtained **ABD** constitutive relationships.

### 2.1. Kinematic relationship between shell and solid formulation

In the proposed procedure the structural scale uses shell elements whereas the substructural and microstructural scales are discretized with solid elements. Consequently, the former scale has a different kinematics than the later scales. In order to define the kinematic relationship between them, it is necessary to study the deformation field on the shell elements, which are used by structural model, and its correlation with the displacement field in the three-dimensional space used by the solid models.

The Kirchhoff–Love (KL) plate theory [21] has been chosen to govern the structural scale behaviour. The KL theory does not take into account the out-of-plane shear of the laminate. Nevertheless, this theory provides a good approximation for laminate with a low thickness-size ratio. KL's theory relies on three kinematic assumptions [6]. These are listed below and represented in Fig. 3:

i Due to bending effects, points belonging to the mid plane only move vertically.
ii After deformation takes place, straight lines perpendicular to the mid-surface remain straight, and perpendicular to the mid surface curvature.
iii The thickness of the plate does not change during a deformation.

Following the above assumptions, it is possible to establish a generic volumetric displacement field for a material point which moves from position $p$ on the undeformed configuration to the position $p'$ on the deformed configuration (see Fig. 3),

$$\begin{aligned} \vec{u}(\vec{x}) = &\quad [u,\ v,\ w\ ]^T\ , \\ u(x,y,z) = &\quad u_r(x,y) + z\ \theta_x(x,y)\,, \\ v(x,y,z) = &\quad v_r(x,y) + z\ \theta_y(x,y)\,, \\ w(x,y) = &\quad w_r(x,y), \end{aligned} \tag{1}$$

where the sub-index $r$ refers to the reference plane. Thus, $u_r$, $v_r$ and $w_r$ are the displacements in $x$, $y$ and $z$ directions of the laminate's reference plane. Given the second condition $(ii)$ both angles of rotation i.e. $\theta_x$ and $\theta_y$ are defined as the partial derivatives of the bending with respect to $x$, $\frac{\partial w}{\partial x}$, and $y$ direction, $\frac{\partial w}{\partial y}$, respectively.

The in-plane strain field $\vec{\varepsilon}_p = [\varepsilon_x, \varepsilon_y, \gamma_{xy}]$ for any point of the laminate is obtained applying the definition of the infinitesimal strain

$$\begin{aligned} \varepsilon_x &= \frac{\partial u}{\partial x} = \underbrace{\frac{\partial u_r}{\partial x}}_{\varepsilon_{r_x}} + z \underbrace{\frac{\partial \theta_x}{\partial x}}_{\kappa_x}\ , \\ \varepsilon_y &= \frac{\partial v}{\partial y} = \underbrace{\frac{\partial v_r}{\partial y}}_{\varepsilon_{r_y}} + z \underbrace{\frac{\partial \theta_y}{\partial y}}_{\kappa_y}\ , \\ \gamma_{xy} &= \frac{\partial u}{\partial y} + \frac{\partial v}{\partial x} = \underbrace{\left(\frac{\partial u_r}{\partial y} + \frac{\partial v_r}{\partial x}\right)}_{\gamma_{r_{xy}}} + z \underbrace{\left(\frac{\partial \theta_x}{\partial y} + \frac{\partial \theta_y}{\partial x}\right)}_{\kappa_{xy}}. \end{aligned} \tag{2}$$

then, Eq. (2) can be written as

$$\vec{\varepsilon}_p = \vec{\varepsilon}_r + z\ \vec{\kappa} \tag{3}$$

where $\vec{\varepsilon}_r = \left[\varepsilon_{r_x}, \varepsilon_{r_y}, \gamma_{r_{xy}}\right]$ is the reference plane strain, and $\vec{\kappa} = [\kappa_x, \kappa_y, \kappa_{xy}]$ contains the curvatures and torsion deformations. Both vectors can be joined in a unique strain vector $\vec{\varepsilon} = [\vec{\varepsilon}_r, \vec{\kappa}]$.

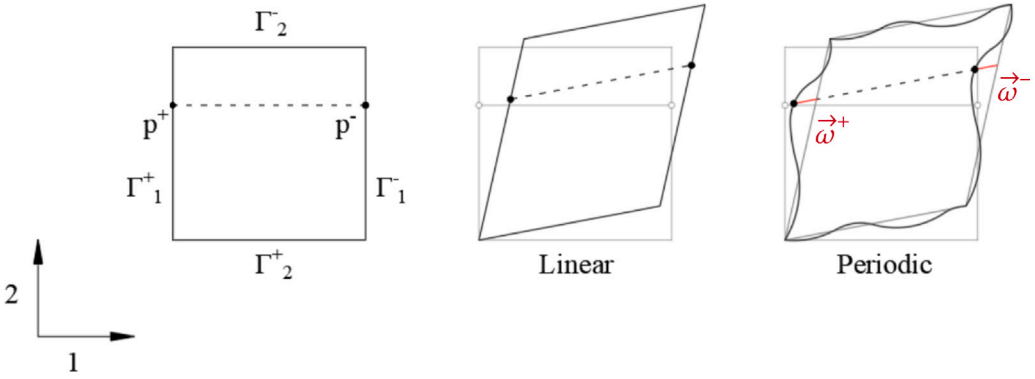


**Fig. 4.** 2D representation of Linear and Periodic boundary conditions.

Integrating Eq. (3) the full three-dimensional displacement field at the subscale level is obtained. Appendix shows the integration procedure followed to obtain the displacement vector $\vec{u}_\mu = [u_\mu, v_\mu, w_\mu]$. The final expression of this displacement is:

$$\begin{aligned} u_\mu(\vec{\varepsilon}, \vec{x}_\mu) &= \varepsilon_{r_x} x_\mu + \frac{\gamma_{r_{xy}}}{2} y_\mu + \kappa_x z_\mu x_\mu + \frac{\kappa_{xy}}{2} z_\mu y_\mu + \omega_x(\vec{x}_\mu), \\ v_\mu(\vec{\varepsilon}, \vec{x}_\mu) &= \varepsilon_{r_y} y_\mu + \frac{\gamma_{r_{xy}}}{2} x_\mu + \kappa_y z_\mu y_\mu + \frac{\kappa_{xy}}{2} z_\mu x_\mu + \omega_y(\vec{x}_\mu), \\ w_\mu(\vec{\varepsilon}, \vec{x}_\mu) &= \frac{\kappa_x}{2} x_\mu^2 + \frac{\kappa_y}{2} y_\mu^2 + \kappa_{xy} x_\mu y_\mu + \omega_z(\vec{x}_\mu), \end{aligned} \tag{4}$$

where $\mu$ refers to the microstructural and substructural scales.

### 2.2. Second order homogenization formulation

The homogenization process aims to define the characteristic behaviour of the subscales when subjected to a strain given by the structural model. In order to induce a structural strain state, a set of displacements are imposed on the boundaries of the subscale models.

When the lengths of the subscales models cannot be considered infinitesimal compared to the structure under study, the linear relationship between the first order deformation gradient $\mathbf{F}$ and the subscale boundary displacements, is no longer fulfilled. This is even more accentuated when the microstructural model represents the total thickness of the laminate. Therefore, it is not possible to use a first-order homogenization to define this relationship.

This phenomenon can be appreciated when studying a solid under bending. If the microstructure is infinitely smaller than the body under study, it will be subjected to pure traction or compression depending on the point studied with respect to the neutral plane. However, as the size of the microstructure increases, the uniformity of traction or compression is lost as the bending has to be taken into account in the microstructure itself. This is shown in the work by Otero et al. [22].

In order to capture the variation of the deformation the second order deformation gradient, ${}^3\mathbf{G}$, must be taken into account. This is introduced by expanding the Taylor series of the displacement at the microstructural and substructural scales

$$\vec{u}_\mu = (\mathbf{F} - \mathbf{I}) \cdot \vec{x}_\mu + \frac{1}{2} \cdot \vec{x}_\mu^{\mathbf{T}} \cdot {}^3\mathbf{G} \cdot \vec{x}_\mu + \vec{\omega}, \tag{5}$$

where the term $\vec{\omega}$ is the displacement fluctuation field.

According to the average theorem, initially introduced by Hill at [23], the deformation gradient $\mathbf{F}$ on any point of the structural scale model must agree with the average of the strain gradient on their representative subscale volume. The same relationship also applies for the second order deformation gradient [24]. Both relationship are expressed as

$$\mathbf{F} \equiv \frac{1}{|\Omega|} \int_\Omega \mathbf{F}_\mu d\Omega \qquad {}^3\mathbf{G} \equiv \frac{1}{|\Omega|} \int_\Omega {}^3\mathbf{G}_\mu d\Omega, \tag{6}$$

where $\Omega$ stands for the volume of the subscales models. Using the displacement expression shown in Eq. (4), the first and second order deformation gradient tensors can be derived by means of the gradient operator $\nabla = (\frac{\partial}{\partial x_1}, \dots, \frac{\partial}{\partial x_n})$ following

$$\mathbf{F} = \mathbf{I} + \nabla \vec{u}_\mu = \mathbf{I} + \begin{bmatrix} \varepsilon_{r_x} + \kappa_x z & \frac{\gamma_{r_{xy}}}{2} + \frac{\kappa_{xy} z}{2} & \kappa_x x + \frac{\kappa_{xy} y}{2} \\ \frac{\gamma_{r_{xy}}}{2} + \frac{\kappa_{xy} z}{2} & \varepsilon_{r_y} + \kappa_y z & \kappa_y y + \frac{\kappa_{xy} x}{2} \\ -\kappa_x x - \frac{\kappa_{xy} y}{2} & -\kappa_y y - \frac{\kappa_{xy} x}{2} & 0 \end{bmatrix} \tag{7}$$

and

$${}^3\mathbf{G} = \nabla \mathbf{F} = \left\{ \frac{\partial(\mathbf{F})}{\partial x}, \frac{\partial(\mathbf{F})}{\partial y}, \frac{\partial(\mathbf{F})}{\partial z} \right\} =$$

$$\left\{ \begin{bmatrix} 0 & 0 & \kappa_x \\ 0 & 0 & \kappa_{xy}/2 \\ -\kappa_x & -\kappa_{xy}/2 & 0 \end{bmatrix}, \begin{bmatrix} 0 & 0 & \kappa_{xy}/2 \\ 0 & 0 & \kappa_y \\ -\kappa_{xy}/2 & -\kappa_y & 0 \end{bmatrix}, \begin{bmatrix} \kappa_x & \kappa_{xy}/2 & 0 \\ \kappa_{xy}/2 & \kappa_y & 0 \\ 0 & 0 & 0 \end{bmatrix} \right\} \tag{8}$$

To satisfy the average strain theorem, written in Eq. (6), some restriction on the displacement fluctuation field must be imposed. The most common restriction on $\vec{\omega}$ is applied at the boundaries of the subscales models, and they are commonly known as Linear and Periodic Boundary Conditions (BC). Fig. 4 shows an example of a 2D microstructural scale model, and the obtained admissible deformations depending on the boundary condition imposed in it. The Linear BC is defined by imposing zero fluctuations on the boundaries, i.e. $\vec{\omega} = 0$,

$$\vec{u}_\mu = (\mathbf{F} - \mathbf{I}) \cdot \vec{x}_\mu + \frac{1}{2} \cdot \vec{x}_\mu^{\mathbf{T}} \cdot {}^3\mathbf{G} \cdot \vec{x}_\mu \tag{9}$$

for any $\vec{x}_\mu \in \Gamma$.

The Periodic BC is obtained when $\vec{\omega}^+ = \vec{\omega}^-$ for all points aligned and located on opposite faces (see Fig. 4), which is imposed with the following displacements in the boundary,

$$\begin{aligned} \vec{u}_\mu{}^+ - \vec{u}_\mu{}^- = (\mathbf{F} - \mathbf{I}) \cdot (\vec{x}_\mu{}^+ - \vec{x}_\mu{}^-) \\ + \frac{1}{2} \cdot (\vec{x}_\mu{}^+ - \vec{x}_\mu{}^-)^{\mathbf{T}} \cdot {}^3\mathbf{G} \cdot (\vec{x}_\mu{}^+ - \vec{x}_\mu{}^-) \end{aligned} \tag{10}$$

for $\forall$ pairs $\{p^+, p^-\} \in \Gamma$.

#### 2.2.1. Mixed boundary conditions

As it has been previously stated, this work will use either microstructural or substructural models of the laminate in order to obtain the material performance to be used in the structural model. The characteristics of these models require using different boundary conditions at the different faces of the microstructure or substructure, as it is

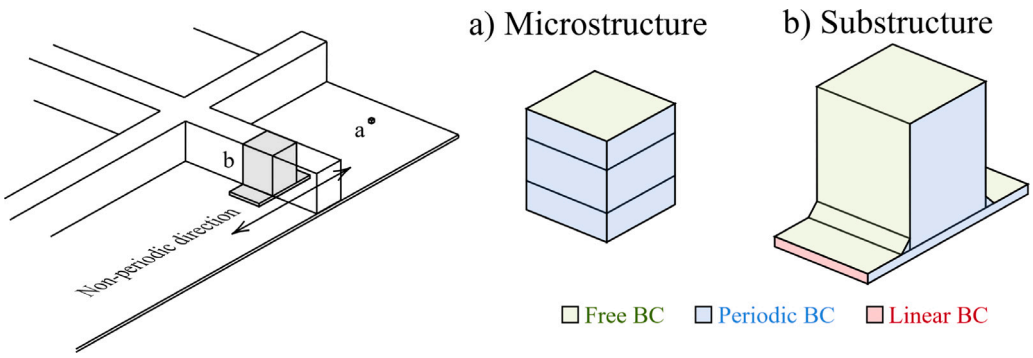


**Fig. 5.** Transition's periodical and non-periodical faces.

shown in Fig. 5. The specific mixed boundary conditions required for each case are described hereafter.

**Microstructural boundary conditions**

The microstructure defined in the developed methodology considers the whole laminate thickness, as can be seen on Fig. 5. Since there is no periodicity in the out-of-plane direction, the model is free to deform along this axis. This geometric feature must be taken into account when the boundary value problem is formulated. For this subscale the boundary conditions that suit the best are the following: Periodic boundary condition for the two pair faces in the in-plane directions (blue faces on Fig. 5), and Free boundary conditions for the upper and lower face on thickness direction (green faces on this same figure).

It should be noted that when working with a second order homogenization formulation, the position of the microstructural coordinate system must be consistent with the reference system used to define the displacement field in the structural model.

**Substructural mixed boundary conditions**

Substructural models are used to characterize transitions, reinforcements or irregularities of the laminate. The particularity of this case, compared with the previous one, is the lost of the periodicity in one pair of faces on the in-plane. Fig. 5 represents a substructure reinforcement example. The substructural model shown only presents periodicity in one in-plane direction meanwhile in the other is lost.

For this substructural scale a combination of Periodic, Linear and Free boundary conditions is proposed. Periodic boundary conditions still apply in the in-plane direction where the geometric periodicity remains (blue faces on Fig. 5). Linear boundary condition are applied in the perpendicular in-plane direction, where there is no periodicity (red faces). Finally, Free boundary conditions are used in the upper and lower face on thickness direction (green faces).

The length of the substructural model of the non-periodic direction needs to be large enough due to the Linear boundary conditions imposed on it. The purpose of this is to minimize the edged effect on the obtained stresses state of the analysed substructure. Following the Saint-Venant principle [25] the optimum length varies according to the thickness. The greater the thickness, the longer the substructural model has to be.

### 2.2.2. Laminate stiffness matrix

The laminate stiffness matrix (**ABD**) is obtained either from the microstructure model or the substructure model by means of an homogenization procedure. This is done by applying the six different pure deformation states .i.e $\vec{\varepsilon} = 0$ less $\vec{\varepsilon}_i$ for $i = 1, 2, \dots, 6$, and computing its associated displacement field with Eq. (4). Then, the boundary value problem on each subscales is solved with the specific boundary conditions explained previously. This generates six different stress states at the subscales. Applying the Hill–Mandel principle [13,22], it can be obtained the following force per unit length $\vec{N} = \left[N_x, N_y, N_{xy}\right]$ and moment per unit length $\vec{M} = \left[M_x, M_y, M_{xy}\right]$ as

$$\vec{N} = \frac{1}{A_\mu} \int_\Omega \vec{\sigma}_\mu \, d\Omega \tag{11}$$

and

$$\vec{M} = \frac{1}{A_\mu} \int_\Omega \vec{\sigma}_\mu \, z \, d\Omega \tag{12}$$

where $\vec{\sigma} = \left[\sigma_x, \sigma_y, \sigma_{xy}\right]$ and $A_\mu$ is the area of the reference plane at the subscales models. The **ABD** constitutive matrix is assembled combining the resulting $\vec{N}$ and $\vec{M}$ for each pure deformation states. This stiffness matrix is the one required by the shell elements at the structural model.

## 3. Implementation workflow

The implementation of the proposed formulation has been carried out for linear elastic problems. A brief description of the workflow for the definition and resolution of these kind of analysis is given below.

The first step consists in assembling the stiffness matrix of each subscale model. For this, it is necessary to define the models geometry, and the constitutive behaviour of their composing materials. Every subscale model is subjected to its six pure strain states corresponding to each one of the deformations components as shown in Fig. 2. This is done computing the corresponding displacement fields with Eq. (4) for each one of the pure strain states and applying the BCs described in Section 2.2.1 according to the model type and the periodicity of its faces. Then the homogenization procedure described in Section 2.2.2 is applied for each one of these pure strain which leads to the constitutive relationship **ABD** for each subscale model.

Finally the analysis of the shell structural model can be performed conventionally. Thus, the obtained **ABD** relationships are assigned to each region of the geometry and the loads and boundary conditions are applied over the structural model. After the analysis has been completed, detailed representations of the stresses and strains on the corresponding microstructure and substructure models can be obtained.

To this end it is necessary to extract the deformation state of each one of the points of interest in the structural model. Then the associated displacement field for each one of these points is obtained by means of Eq. (4). These fields can be applied to the subscale models in the same way as it is done during the homogenization process, i.e. with the corresponding boundary conditions for each model, leading to a detailed representation of the strains and stresses for a given structural point in the solid model.

## 4. Numerical example

This section presents a numerical example to show the capabilities of the proposed formulation when analysing real laminate composite structures. To validate the whole procedure, two models are defined, a solid structural model, used as a reference, and its equivalent multiscale structural shell model with the same geometry. Both models reproduce an structure of composite laminate with a central omega reinforcement subjected to a tensile load.

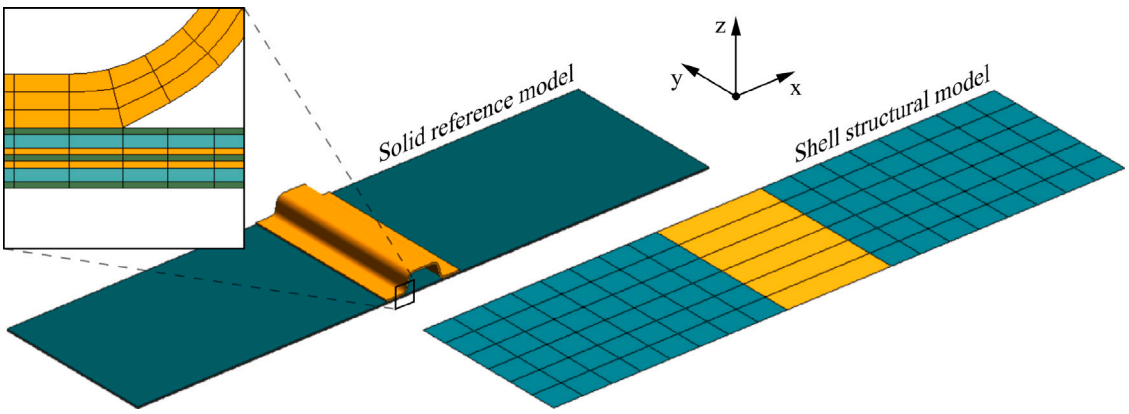


**Fig. 6.** Solid reference model and its analogous shell structural model.

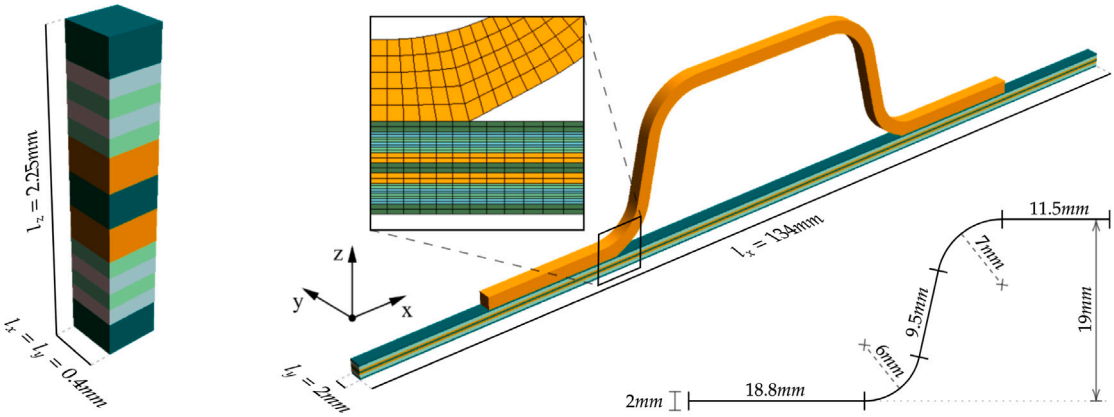


(a) Laminate microstructure.

(b) Omega reinforcement substructure.

**Fig. 7.** Subscale models.

**Table 1**
Properties of the unidirectional long carbon fibre reinforced epoxy (AS4-3501-6).

| Unidirectional composite properties | |
|---|---|
| $E_1$ [MPa] | 142,000 |
| $E_2 = E_3$ [MPa] | 10,300 |
| $\nu_{12} = \nu_{13}$ | 0.27 |
| $\nu_{23}$ | 0.40 |
| $G_{12} = G_{13} = G_{23}$ [MPa] | 7,200 |

**Table 2**
Macro-models meshes.

| Mesh data | | | |
|---|---|---|---|
| Model | # elem. | # nodes | # DOFs |
| Solid structural | 102,400 | 465,800 | 2,329,000 |
| Shell structural | 102 | 126 | 630 |
| Substructure | 13,662 | 76,274 | 381,370 |
| Microstructure | 512 | 2,945 | 14,725 |

### 4.1. Model description and applied load

The studied specimen has a total length of 740 mm in longitudinal direction and 200 mm in transversal direction. The stacking sequence of the laminate is given by $[0_2, \pm 45_2, 90_2, 0]_s$ where each layer is 0.125 mm thick. All layers are a unidirectional carbon fibre composite with the properties listed in Table 1. The central reinforcement consists in a omega profile using the same composite material but containing only fibres aligned in its longitudinal direction and with a total thickness of 2 mm. The dimensions of its geometry are depicted in Fig. 7(a).

The solid structural model is meshed with Serendipity hexahedral elements of 20 nodes each and integrated with a $3 \times 3 \times 3$ points quadrature [26]. Each layer has been discretized separately, as can be seen in the detail in Fig. 6, which ensure a high level of accuracy [6]. The computational cost of this kind of elements is high but they are able to capture the strain distribution with high accuracy in the whole structural model (laminate and omega reinforcement). In order to establish a direct comparison between the obtained results, the microstructural and substructural models are meshed using the same kind of finite elements. Similarly to the structural model each layer has been discretized separately in their out of plane direction but in this case with more than one element, as can be seen in the mesh representation of Fig. 7(b).

The structural shell model is meshed with MZC rectangular elements [27], capable of reproducing the Kirchhoff kinematics, in addition the membrane behaviour has been added what introduces the in-plane phenomena [6]. Its integration is performed with a $2 \times 2$ points quadrature. Table 2 shows a comparison between the total number of nodes, elements and degrees of freedom for each model.

The tensile load is applied over the structural models as an imposed displacement that extends the longitudinal length a 1% of its total length. This displacement is applied at both ends, locking at the same time these in all their directions. In the structural shell model, all rotations are also blocked at both ends.

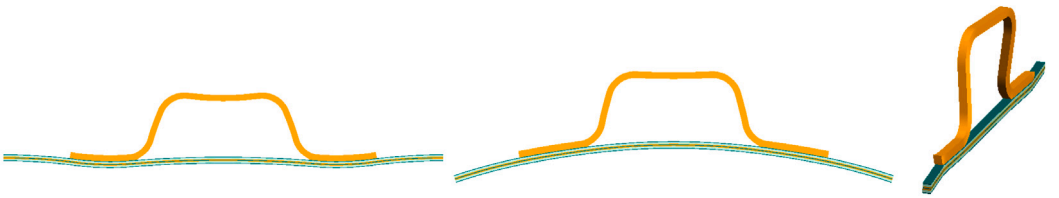

(a) $\varepsilon_{r_x} = 0.01$ (b) $\kappa_x = 0.01$ (c) $\gamma_{r_{xy}} = 0.01$

**Fig. 8.** Reinforcement substructure under homogenization procedure (Magnified ×10, ×1, ×50 respectively).

### 4.2. Subscale models. Geometry and stiffness matrix

The selected geometries of the subscale models are represented in Fig. 7. Fig. 7(a) shows the microstructural model of the continuous laminate and Fig. 7(b) shows the corresponding substructural model of the omega profile.

The constitutive matrix **ABD** is obtained following the homogenization procedure described in Section 2.2.2. The constitutive matrix obtained for the microstructure of the laminate is shown in Eq. (13). This **ABD** matrix is exactly the same that is obtained with the Classical Lamination Theory (CLT) [7], which validates the result obtained and the procedure developed. Although in this case the use of a microstructure to obtain this matrix is proved unnecessary, this will not the case when analysing laminates with a more complex microstructure that cannot be captured by the CLT, such as sandwich materials with a honeycomb core.

The constitutive matrix for the substructure is shown in Eq. (14). In this case, this matrix cannot be obtained analytically. As can be seen, a non-zero **B** submatrix (top-right and bottom-left) is obtained due to the presence of the Omega reinforcement. The comparison of Eq. (14) with Eq. (13) shows a substantial increase in stiffness in the direction of the Omega, defined along y-direction according to Fig. 7. In this direction there is a three-times higher in-plane stiffness (submatrix **A**) and a three orders of magnitude gain on bending stiffness (submatrix **D**). The coupling that introduces the **B** submatrix can be appreciated in Fig. 8(a), where it is shown the deformation of the substructure during the homogenization procedure for a structural strain of $\varepsilon_{r_x} = 0.01$.

$$\mathbf{ABD}_{ms} = \left[\begin{array}{ccc|ccc} 159119 & 35970 & 0 & 0 & 0 & 0 \\ 35970 & 126019 & 0 & 0 & 0 & 0 \\ 0 & 0 & 45879 & 0 & 0 & 0 \\ \hline 0 & 0 & 0 & 91572 & 14865 & 2585 \\ 0 & 0 & 0 & 14865 & 29337 & 2585 \\ 0 & 0 & 0 & 2585 & 2585 & 19046 \end{array}\right] \tag{13}$$

$$\mathbf{ABD}_{ss} = \left[\begin{array}{ccc|ccc} 162507 & 36905 & 0 & 8077 & 2181 & 0 \\ 36905 & 381581 & 0 & 2181 & 2911311 & 0 \\ 0 & 0 & 53201 & 0 & 0 & 74520 \\ \hline 8077 & 2181 & 0 & 121558 & 22966 & 2569 \\ 2181 & 2911311 & 0 & 22966 & 53844221 & 2581 \\ 0 & 0 & 74520 & 2569 & 2581 & 1156870 \end{array}\right] \tag{14}$$

### 4.3. Results obtained

The results obtained for the structural solid model and the equivalent structural shell model are compared below. Fig. 9 shows the displacement field comparison in directions $x$, $y$ and $z$. The displacement fields represented for the volumetric models correspond to the mid plane.

A very good correlation can be appreciated between the displacement field of both models as the resultant displacement fields only differ on the edges of the laminate next to the transition elements. In these edges, the stiffness difference between the shell and the omega profile generates a variation in the result of the solid model that is not captured by the shell one, which provides more regular and smooth results. This behaviour cannot be captured by the structural shell model, as shell elements only can reproduce periodic behaviour in this direction. Despite the aforementioned difference, the agreement on the displacements validates the methodology and shows the need of including the effects produced by laminate discontinuities (such the omega profile) in the laminate response, as these modify substantially the displacement field and, therefore, the performance of the whole structure.

The proposed procedure is able to analyze the local performance of the subscales using the strain states provided by the structural model. Using the strain at point $A$ (Fig. 9) in the shell model, and applying it on the substructural model (Fig. 7(b)), leads to the stress distribution shown in the right hand side of Fig. 10. The stresses obtained in equivalent location of the solid reference model are shown in the left hand side of Fig. 10 in order to establish a direct comparison.

The obtained results in both models, shown in Figure and Fig. 10 and 3 respectively, are in good agreement. In the first place the values of the $x$-direction stresses are almost identical. As it is also identical the distribution of these stresses in the laminate layers, and in the reinforcement. As for the stresses obtained in $y$-direction, they are also very similar in their distribution in the laminate layers and omega reinforcement, however the solid model shows larger values in some regions as can be seen in the figures of point's "a" in Table 3. This phenomena is mainly caused by the sensibility of $y$-direction stresses to the $\kappa_y$ curvature. The height of the substructure and the high stiffness of the composite material leads to very sharp changes on the stress distribution for a small variations of $\kappa_y$.

Having proved that the results provided by the proposed methodology are in a good agreement with the ones provided by a detailed 3D model, the other outcome that has to be highlighted is the reduction of the computational cost of the analysis. The direct comparison between the number of degrees of freedom on the structural models, solid and shell, already reflects the significant savings. As it can be seen in Table 2 the total number of DOF is four orders of magnitude lower in the shell model, a pattern that also holds true when it comes to comparing the computational time. Therefore using the proposed multiscale method larger structures can be analyzed much faster than using a conventional solid model.

On the other hand, the computational cost of homogenization procedure is low and only takes place once at the beginning of the simulation. In addition the subscale models have a much smaller number of elements in comparison with the structural model discretized with a similar mesh (see Table 2). Moreover, once homogenized, the **ABD** matrix of each subscale models can be stored and reused, thus bypassing the homogenization procedure and moving directly to the resolution of the structural shell model.

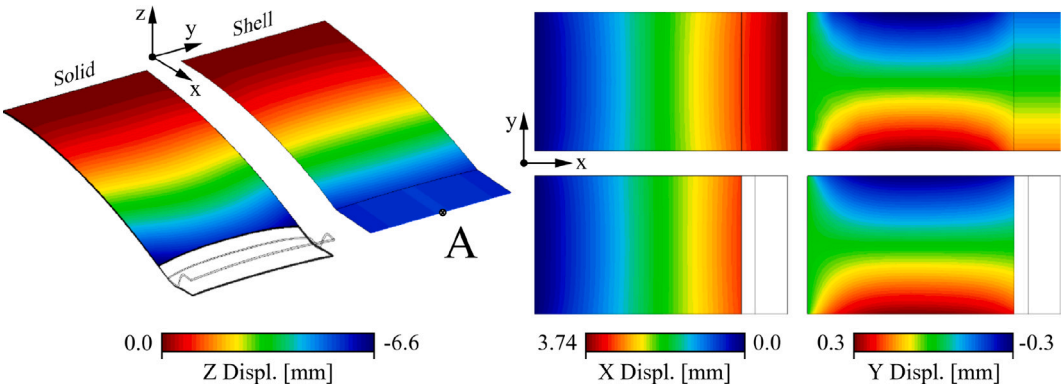


**Fig. 9.** Comparison between the displacement fields from the solid reference and shell structural models.

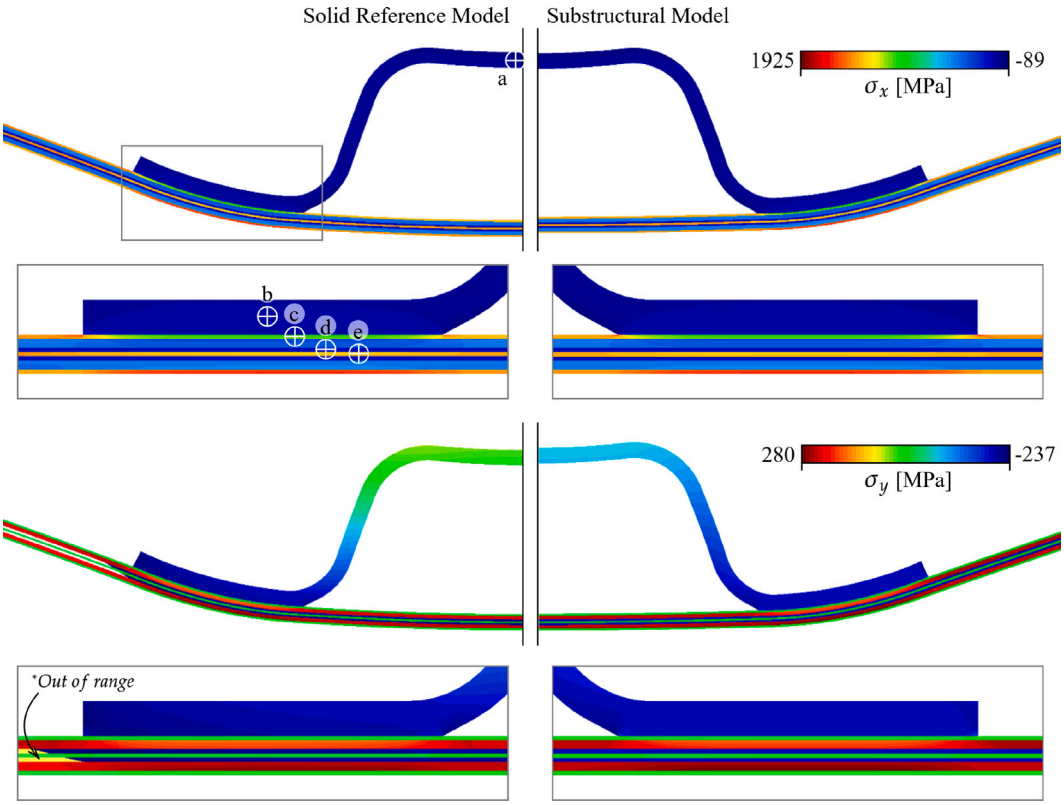


**Fig. 10.** Comparison between the stresses in the $x$ and $y$ directions on the solid reference model and the corresponding substructure (Magnified ×10).

**Table 3**
Stress value in the indicated points of Fig. 10 [MPa].

| | a | | b | | c | | d | | e | |
|---|---|---|---|---|---|---|---|---|---|---|
| | $\sigma_x$ | $\sigma_y$ | $\sigma_x$ | $\sigma_y$ | $\sigma_x$ | $\sigma_y$ | $\sigma_x$ | $\sigma_y$ | $\sigma_x$ | $\sigma_y$ |
| Solid Ref. Model | 1.7 | 39.0 | 53.4 | −202.1 | 1019.9 | 3.6 | 84.7 | −209.6 | 1302.9 | 8.1 |
| Substruc. Model | 0.6 | −60.5 | 47.5 | −188.3 | 1024.4 | 5.3 | 84.5 | −190.4 | 1304.4 | 9.8 |

## 5. Conclusions

This paper presents a new theoretical framework, and its numerical implementation, for the analysis of composite laminar structures. The proposed procedure obtains the mechanical performance of the shell structural model, either in the continuous laminate zones or in any possible irregularity existing in it, from the numerical analysis of a microstructure and a substructure, respectively. In addition, a suitable combination of mixed boundary conditions is proposed for the study of the subscale models in which periodicity conditions are lost.

The validation example included has proved the accuracy of the procedure proposed, showing that the results obtained with it are practically identical to the results obtained with a detailed 3D solid model of the structure; and has also shown the capabilities of the method, and the results that can be obtained with it. Following the proposed approach, it is possible not only to obtain a close approximation of the mechanical behaviour of complex laminate configurations and laminate irregularities (e.g. transition reinforcements or changes in the laminate thickness) with a high level of detail, but also to accurately predict their stiffness participation in the overall structure.

Despite all the advantages provided by the formulation developed, due to the assumptions made during the homogenization procedure, this approach has also some limitations. A continuous state of deformation is considered on the subscale models when defining their constitutive ABD matrix. For this reason, when the structural model shows pronounced changes in the deformation field, the obtained result may have some slight variations in comparison the real kinematics.

Nevertheless, having the complete macro-structure analysed with the shell elements defined in this work, provides the high result accuracy proved in the validation example with a minimal computational cost in terms of computing time and required memory. This capability opens a new path on the numerical analysis of large laminate composite structures, which now can take into account the effects of different laminate configurations and irregularities, in the overall structural response. This capability is expected to improve the design of laminate structures such as airplanes and ships, increasing their safety, reducing their weight, and minimizing their environmental impact.

## Declaration of competing interest

Regarding the submission of the manuscript entitled "Multi-scale procedure for the mechanical analysis of composite laminate structures considering mixed boundary conditions" to the journal Composite Structures, the authors want to state that we do have no conflicts of interest to disclose.

## Data availability

No data was used for the research described in the article

## Acknowledgements

This work has received funding from the European Union's Horizon 2020 research and innovation programme under grant agreement № 101006860 (FIBRE4YARDS project) and under grant agreement № 952966 (FIBREGY project). In addition, this research work is framed within an FI doctoral grant awarded by the Generalitat de Catalunya, Spain and co-financed jointly with the European Union. These supports are gratefully acknowledged.

## Appendix. Integration of the deformation field

In this appendix the in-plane strain at the structural level defined in Eq. (2) is used to obtain the displacement field given at the subscales level. Based on the principle of scales separation, the structural strains can be considered constant at the subscales domain. Under this assumption, the displacement field at the subscale level is obtained with the following expressions:

$$\begin{aligned} u_\mu(\vec{\varepsilon},\vec{x}_\mu) &= u^\varepsilon_\mu(\vec{\varepsilon},\vec{x}_\mu) + \omega_x(\vec{x}_\mu) \\ &= u^\mu_r(\vec{\varepsilon}_r,\vec{x}_\mu) + u^\mu_\kappa(\vec{\kappa},\vec{x}_\mu) + \omega_x(\vec{x}_\mu) \\ v_\mu(\vec{\varepsilon},\vec{x}_\mu) &= v^\varepsilon_\mu(\vec{\varepsilon},\vec{x}_\mu) + \omega_y(\vec{x}_\mu) \\ &= v^\mu_r(\vec{\varepsilon}_r,\vec{x}_\mu) + v^\mu_\kappa(\vec{\kappa},\vec{x}_\mu) + \omega_y(\vec{x}_\mu) \\ w_\mu(\vec{\varepsilon},\vec{x}_\mu) &= w^\varepsilon_\mu(\vec{\varepsilon},\vec{x}_\mu) + \omega_z(\vec{x}_\mu) \\ &= w^\mu_\kappa(\vec{\kappa},\vec{x}_\mu) + \omega_z(\vec{x}_\mu). \end{aligned} \tag{A.1}$$

Where $\vec{u}^\mu_r = \left[u^\mu_r, v^\mu_r\right]$ is the part of the displacements given by the strains in the reference plane, $\vec{u}^\mu_\kappa = \left[u^\mu_\kappa, v^\mu_\kappa, w^\mu_\kappa\right]$ is the part induced by the curvature effect and $\vec{\omega} = \left[\omega_x, \omega_y, \omega_z\right]$ is the displacement fluctuation field at the micro or substructural scales [22].

The different components of the proposed displacement field are obtained using differential analysis. Assuming an infinitesimal volume, the variation of $u^\varepsilon_\mu$ is given by

$$du^\varepsilon_\mu = \frac{\partial u^\mu_r(\vec{\varepsilon}_r,\vec{x}_\mu)}{\partial \vec{x}_\mu} d\vec{x}_\mu + \frac{u^\mu_\kappa(\vec{\kappa},\vec{x}_\mu)}{\partial \vec{x}_\mu} d\vec{x}_\mu \tag{A.2}$$

where, the first term can be obtained by,

$$\frac{\partial u^\mu_r(\vec{\varepsilon}_r,\vec{x}_\mu)}{\partial \vec{x}_\mu} d\vec{x}_\mu = \frac{\partial u^\mu_r}{\partial x_\mu} dx_\mu + \frac{\partial u^\mu_r}{\partial y_\mu} dy_\mu + \frac{\partial u^\mu_r}{\partial z_\mu} dz_\mu. \tag{A.3}$$

Then, based on the Kirchhoff–Love (KL) theory it is assumed the following:

$$\frac{\partial u^\mu_r}{\partial x_\mu} = \varepsilon_{r_x} \quad ; \quad \frac{\partial u^\mu_r}{\partial y_\mu} = \frac{\gamma_{r_{xy}}}{2} \quad ; \quad \frac{\partial u^\mu_r}{\partial z_\mu} = 0. \tag{A.4}$$

The displacement $u_\mu$ depends on the reference plane strain, and it is integrated as,

$$u^\mu_r = \int_{\partial\Omega_x} \varepsilon_{r_x} dx_\mu + \int_{\partial\Omega_y} \frac{\gamma_{r_{zy}}}{2} dy_\mu = \varepsilon_{r_x} x_\mu + \frac{\gamma_{r_{zy}}}{2} y_\mu. \tag{A.5}$$

A similar procedure is followed for second term of Eq. (A.2)

$$\frac{\partial u^\mu_\kappa(\vec{\kappa},\vec{x}_\mu)}{\partial \vec{x}_\mu} d\vec{x}_\mu = \frac{\partial u^\mu_\kappa}{\partial x_\mu} dx_\mu + \frac{\partial u^\mu_\kappa}{\partial y_\mu} dy_\mu + \frac{\partial u^\mu_\kappa}{\partial z_\mu} dz_\mu, \tag{A.6}$$

and, on the KL theory:

$$\frac{\partial u^\mu_\kappa}{\partial x_\mu} = \kappa_x z_\mu \quad ; \quad \frac{\partial u^\mu_\kappa}{\partial y_\mu} = \frac{\kappa_{xy}}{2} z_\mu \quad ; \quad \frac{\partial u^\mu_\kappa}{\partial z_\mu} = 0. \tag{A.7}$$

The displacement $u_\mu$ depends on the out of plane strain, and it is integrated as,

$$u^\mu_\kappa = \int_{\partial\Omega_x} \kappa_x z_\mu dx_\mu + \int_{\partial\Omega_y} \frac{\kappa_{xy}}{2} z_\mu dy_\mu = \kappa_x z_\mu x_\mu + \frac{\kappa_{xy}}{2} z_\mu y_\mu. \tag{A.8}$$

The same procedure described for $u_n u$ is followed to obtain the displacement in $y$ direction i.e. $v_\mu$.

The last term to be computed are the out-of-plane displacements $w_\kappa$ due to the curvatures $\kappa_x$ and $\kappa_y$ are calculated based on the definition of the curvatures, for both $x$ and $y$ directions.

$$dw^\varepsilon_\mu = \frac{\partial w^\mu_\kappa(\vec{\kappa},\vec{x}_\mu)}{\partial \vec{x}_\mu} d\vec{x}_\mu = \frac{\partial w^\mu_\kappa}{\partial x_\mu} dx_\mu + \frac{\partial w^\mu_\kappa}{\partial y_\mu} dy_\mu + \frac{\partial w^\mu_\kappa}{\partial z_\mu} dz_\mu \tag{A.9}$$

where $\frac{\partial w^\mu_\kappa}{\partial z_\mu}$ is equal to zero according to KL theory.

The other two derivatives of $w$ in expression (A.9) can be obtained from the definition of an infinitesimal change in the angles of rotation:

$$\begin{aligned} d\theta_x &= \frac{\partial \theta_x}{\partial x_\mu} dx_\mu + \frac{\partial \theta_x}{\partial y_\mu} dy_\mu \\ d\theta_y &= \frac{\partial \theta_y}{\partial y_\mu} dy_\mu + \frac{\partial \theta_y}{\partial x_\mu} dx_\mu, \end{aligned} \tag{A.10}$$

where,

$$\frac{\partial \theta_x}{\partial x_\mu} = \kappa_x \quad ; \quad \frac{\partial \theta_y}{\partial y_\mu} = \kappa_y \quad ; \quad \frac{\partial \theta_x}{\partial y_\mu} = \frac{\partial \theta_y}{\partial x_\mu} = \frac{\kappa_{xy}}{2}. \tag{A.11}$$

Then, integrating the previous equations and using the definition of the rotations,

$$\begin{aligned} \theta_x &= \int_{\partial\Omega_x} \kappa_x \, dx_\mu + \int_{\partial\Omega_y} \frac{\kappa_{xy}}{2} \, dy_\mu = \frac{\partial w^\mu_\kappa}{\partial x_\mu} \\ \theta_y &= \int_{\partial\Omega_y} \kappa_y \, dy_\mu + \int_{\partial\Omega_x} \frac{\kappa_{xy}}{2} \, dx_\mu = \frac{\partial w^\mu_\kappa}{\partial y_\mu} \end{aligned} \tag{A.12}$$

Finally, replacing (A.12) to (A.9) and integration the resulting expression leads to the $w^\varepsilon_\mu$ definition

$$w^\varepsilon_\mu = \int_{\partial\Omega_x}\int_{\partial\Omega_x} \kappa_x dx_\mu dx_\mu + \int_{\partial\Omega_y}\int_{\partial\Omega_y} \kappa_y dy_\mu dy_\mu + \int_{\partial\Omega_y}\int_{\partial\Omega_x} \kappa_{xy} dx_\mu dy_\mu \tag{A.13}$$

$$= \frac{\kappa_x}{2} x^2_\mu + \frac{\kappa_y}{2} y^2_\mu + \kappa_{xy} x_\mu y_\mu \tag{A.14}$$

Rearranging all expressions derived in this annex, the displacement field $\vec{u} = [u_\mu, v_\mu, w_\mu]$ for a given structural deformation state can be

calculated as the addition of the following terms,

$$
\begin{aligned}
u_\mu(\vec{\varepsilon},\vec{x}_\mu) &= \varepsilon_{r_x} x_\mu + \frac{\gamma_{r_{xy}}}{2} y_\mu + \kappa_x z_\mu x_\mu + \frac{\kappa_{xy}}{2} z_\mu y_\mu + \omega_x(\vec{x}_\mu),\\
v_\mu(\vec{\varepsilon},\vec{x}_\mu) &= \varepsilon_{r_y} y_\mu + \frac{\gamma_{r_{xy}}}{2} x_\mu + \kappa_y z_\mu y_\mu + \frac{\kappa_{xy}}{2} z_\mu x_\mu + \omega_y(\vec{x}_\mu),\\
w_\mu(\vec{\varepsilon},\vec{x}_\mu) &= \frac{\kappa_x}{2} x_\mu^2 + \frac{\kappa_y}{2} y_\mu^2 + \kappa_{xy} x_\mu y_\mu + \omega_z(\vec{x}_\mu).
\end{aligned}
\tag{A.15}
$$

## References


[1] Banat D, Mania RJ. Stability and strength analysis of thin-walled GLARE composite profiles subjected to axial loading. Compos Struct 2019;212. http://dx.doi.org/10.1016/j.compstruct.2019.01.052.

[2] Jurado A, García C, Sanchez E. FIBRESHIP, the greatest challenge of using composite materials for the construction of large-length ships. Rev Mater Compuestos 2022. http://dx.doi.org/10.23967/R.MATCOMP.2022.07.041.

[3] Thomsen OT. Sandwich materials for wind turbine blades — present and future. J Sandw Struct Mater 2009;11. http://dx.doi.org/10.1177/1099636208099710.

[4] Hiken A. The evolution of the composite fuselage — A manufacturing perspective. SAE Int J Aerosp 2017;10. http://dx.doi.org/10.4271/2017-01-2154.

[5] Turon F, Otero F, Martinez X. Structural analyses of orthogrid fuselage panel for integrated ku-band satcom antenna. In: European conference on multifunctional structures. 2019, http://dx.doi.org/10.23967/emus.2019.016.

[6] Oñate E. Structural analysis with the finite element method: Linear statics. Beams, plates and shells, vol. 2, Springer; 2013.

[7] Barbero EJ. Introduction to composite materials design. 2nd ed. 2010.

[8] Sorrenti M, Sciuva MD. An enhancement of the warping shear functions of refined zigzag theory. J Appl Mech Trans ASME 2021;88. http://dx.doi.org/10.1115/1.4050908.

[9] Carrera E, de Miguel AG, Filippi M, Kaleel I, Pagani A, Petrolo M, et al. Global-local plug-in for high-fidelity composite stress analysis in femap/NX nastran. 28, 2019, p. 1121–7. http://dx.doi.org/10.1080/15376494.2019.1655689.

[10] Gruttmann F, Wagner W. A coupled two-scale shell model with applications to layered structures. Internat J Numer Methods Engrg 2013;94. http://dx.doi.org/10.1002/nme.4496.

[11] Massart TJ, Mercatoris BCN, Piezel B, Berke P, Laiarinandrasana L, Thionnet A. Multi-scale modelling of heterogeneous shell structures. Comput Assist Mech Eng Sci 2011;18.

[12] Mallikarachchi HMYC, Pellegrino S. Quasi-static folding and deployment of ultrathin composite tape-spring hinges. J Spacecr Rockets 2011;48. http://dx.doi.org/10.2514/1.47321.

[13] Helfen CE, Diebels S. Computational homogenisation of composite plates: Consideration of the thickness change with a modified projection strategy. Comput Math Appl 2014;67. http://dx.doi.org/10.1016/j.camwa.2013.12.017.

[14] Geers MGD, Coenen EWC, Kouznetsova VG. Multi-scale computational homogenization of structured thin sheets. 15, 2007, http://dx.doi.org/10.1088/0965-0393/15/4/S06,

[15] Coenen EWC, Kouznetsova VG, Geers MGD. A multi-scale computational strategy for structured thin sheets. Int J Mater Form 2008;1. http://dx.doi.org/10.1007/s12289-008-0044-x.

[16] Kouznetsova VG, Geers MGD, Brekelmans WAM. Multi-scale second-order computational homogenization of multi-phase materials: A nested finite element solution strategy. Comput Methods Appl Mech Engrg 2004;193. http://dx.doi.org/10.1016/j.cma.2003.12.073.

[17] Huang Z, Xing Y, Gao Y. Two-scale asymptotic homogenization method for composite Kirchhoff plates with in-plane periodicity. Aerospace 2022;9:751. http://dx.doi.org/10.3390/AEROSPACE9120751.

[18] Cai Y, Xu L, Cheng G. Novel numerical implementation of asymptotic homogenization method for periodic plate structures. Int J Solids Struct 2014;51:284–92. http://dx.doi.org/10.1016/J.IJSOLSTR.2013.10.003.

[19] Ameen MM, Peerlings RHJ, Geers MGD. A quantitative assessment of the scale separation limits of classical and higher-order asymptotic homogenization. Eur J Mech A Solids 2018;71:89–100. http://dx.doi.org/10.1016/J.EUROMECHSOL.2018.02.011.

[20] Martinez X, Oller S, Rastellini F, Barbat AH. A numerical procedure simulating RC structures reinforced with FRP using the serial/parallel mixing theory. Comput Struct 2008;86. http://dx.doi.org/10.1016/j.compstruc.2008.01.007.

[21] Timoshenko SPSP, Woinosky-Krieger S. Theory of plates and shells. 2nd ed. 1964.

[22] Otero F, Oller S, Martinez X. Multiscale computational homogenization: Review and proposal of a new enhanced-first-order method. Arch Comput Methods Eng 2018;25. http://dx.doi.org/10.1007/s11831-016-9205-0.

[23] Hill R. Elastic properties of reinforced solids: Some theoretical principles. J Mech Phys Solids 1963;11(5):357–72. http://dx.doi.org/10.1016/0022-5096(63)90036-X.

[24] Kouznetsova V, Geers MGD, Brekelmans WAM. Multi-scale constitutive modelling of heterogeneous materials with a gradient-enhanced computational homogenization scheme. Internat J Numer Methods Engrg 2002;54:1235–60. http://dx.doi.org/10.1002/NME.541.

[25] Olivella XO, de Saracibar Bosch CA. Continuum mechanics for engineers. Theory and problems, 2017, http://dx.doi.org/10.13140/RG.2.2.25821.20961.

[26] Oñate E. Structural analysis with the finite element method. Basis and solid, vol. 1, Springer; 2009.

[27] Melosh R. Structural analysis of solids. J Struct Div 1963;205–23.